Pattern Recognition 74 (2018) 110–121

Contents lists available at ScienceDirect

Pattern Recognition

journal homepage: www.elsevier.com/locate/patcog

Rotation invariants of vector fields from orthogonal moments

Bo Yang[a], Jitka Kostková[b], Jan Flusser[b,*], Tomáš Suk[b], Roxana Bujack[c]

[a] School of Automation, Northwestern Polytechnical University, 127 West Youyi Road, 710 072 Xi'an Shaanxi, P.R. China
[b] Institute of Information Theory and Automation of the CAS, Pod vodárenskou věží 4, 182 08 Praha 8, Czech Republic
[c] Data Science at Scale Team, Los Alamos National Laboratory, P.O. Box 1663, Los Alamos, NM 87545, USA

ARTICLE INFO

Article history:
Received 31 March 2017
Revised 2 September 2017
Accepted 5 September 2017
Available online 11 September 2017

Keywords:
Vector field
Total rotation
Invariants
Gaussian–Hermite moments
Zernike moments
Numerical stability

ABSTRACT

Vector field images are a type of new multidimensional data that appear in many engineering areas. Although the vector fields can be visualized as images, they differ from graylevel and color images in several aspects. To analyze them, special methods and algorithms must be originally developed or substantially adapted from the traditional image processing area. In this paper, we propose a method for the description and matching of vector field patterns under an unknown rotation of the field. Rotation of a vector field is so-called total rotation, where the action is applied not only on the spatial coordinates but also on the field values. Invariants of vector fields with respect to total rotation constructed from orthogonal Gaussian–Hermite moments and Zernike moments are introduced. Their numerical stability is shown to be better than that of the invariants published so far. We demonstrate their usefulness in a real world template matching application of rotated vector fields.

1. Introduction

In the last decade, an increasing attention has been paid to *vector field* images and to the tools for their analysis. Vector fields arise in mechanical engineering, fluid dynamics, computer vision, meteorology, and many other application areas. They describe particle velocity, wind velocity, optical/motion flow, image gradient, and other phenomena, for instance, flowing water in a pipe, an air flow around an aircraft wing or around a coachwork, or a wind velocity map. Vector fields are obtained as a result of computer processing of standard digital images or videos, numerical solutions of the Navier–Stokes equations, or from real physical measurements (see Fig. 1).

A 2D vector field $\mathbf{f}(\mathbf{x})$ can be mathematically described as a pair of scalar fields (images) $\mathbf{f}(\mathbf{x}) = (f_1(\mathbf{x}), f_2(\mathbf{x}))$. At each point $\mathbf{x} = (x, y)$, the value of $\mathbf{f}(\mathbf{x})$ shows the orientation and the magnitude of a certain vector.

A common task in vector field analysis is the detection of various patterns of interest. It comprises not only detection of singularities such as sinks, vortices, saddle points, vortex-saddle combinations, and double vortices, but also detection of patterns which are not specific but are similar to the pattern stored in the database. For engineers and designers, it is very important to identify these patterns of interest in the flow, because they may increase the friction, vary the pressure, or decrease the speed of the medium, which consequently increases the power and cost necessary to transport it through the pipe or the object through the air or water. We also may just look for an appearance of certain pattern because it may indicate the presence of the physical phenomenon in the fluid we are interested in. The detection of these features is typically accomplished by template matching.[1] Sample templates of these patterns, obtained from similar fields or as a result of a simulation, are stored in the template database and searched in the given field. The search algorithm must be primarily *rotation invariant*, because the particular orientation of the template is unknown (see Fig. 2 for illustration). It is further important that the algorithm is robust with respect to noise in the measurements.

Many template-matching techniques have been developed for scalar images. The key point to avoid a brute-force search is to find rotation-invariant template descriptors. The matching is then performed by a search of all possible template locations (which may be sped-up by a pyramidal representation of the image) and

* Corresponding author.
E-mail addresses: bo.yang@hotmail.fr (B. Yang), kostkova@utia.cas.cz (J. Kostková), flusser@utia.cas.cz (J. Flusser), suk@utia.cas.cz (T. Suk), bujack@lanl.gov (R. Bujack).

[1] If the patterns to be detected were only singularities or other mathematically well-described patterns, we could alternatively use other methods. Template matching is a general method suitable for any pattern which is defined by example rather than by mathematical description.

http://dx.doi.org/10.1016/j.patcog.2017.09.004
0031-3203/

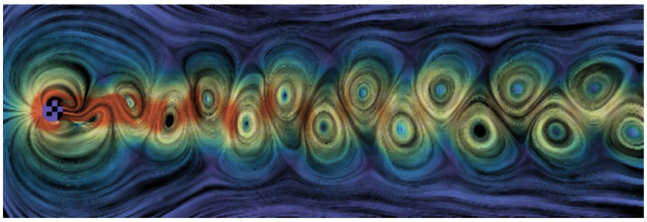

Fig. 1. Fluid flow behind an obstacle. The flow direction is visualized using line integral convolution and the velocity is encoded in the color.

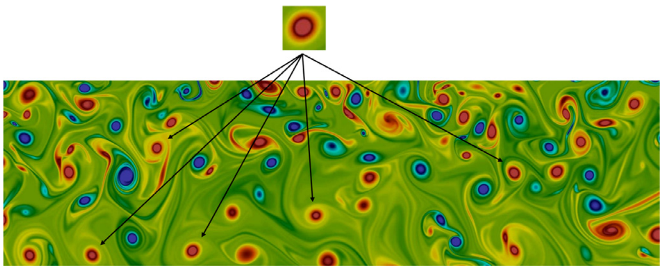

Fig. 2. Vortex detection in a swirling fluid by template matching. The detection method must be invariant to the template orientation.

the matching position is determined as that one which minimizes certain "distance" (usually derived from ℓ_2-norm) in the high-dimensional feature-space of descriptors. The first method of this kind was proposed by Goshtasby [1], who used rotation invariants from geometric moments as the descriptors, but in principle any invariants from any kind of features [2–7] can be used for this purpose.

The methods (or, more precisely, the invariant descriptors) originally designed for scalar images cannot be applied directly to vector fields, because the behavior of a vector field under rotation is substantially different. The rotation of scalar image f by the angle α can be described as

$$f'(\mathbf{x}) = f(\mathbf{R}_{-\alpha} \cdot \mathbf{x}),$$

where

$$\mathbf{R}_\alpha = \begin{pmatrix} \cos\alpha & -\sin\alpha \\ \sin\alpha & \cos\alpha \end{pmatrix}$$

is a rotation matrix. This rotation, called *inner rotation*, affects the spatial coordinates only.

However, when rotating a vector field, the situation is different. The vectors rotate inversely to the in-plane rotation such that their relative orientation to the image content stays constant. The underlying model, which is called *total rotation*, is

$$\mathbf{f}'(\mathbf{x}) = \mathbf{R}_\alpha \mathbf{f}(\mathbf{R}_{-\alpha} \cdot \mathbf{x}).$$

The total rotation of a sample vector field is illustrated in Fig. 3(b) for $\alpha = 22.5°$. Each arrow is rotated around the image center to the new position and its direction is also rotated by the same angle.

In order to implement a rotation-invariant template matching algorithm, we first need to find descriptors that are invariant with respect to the total rotation of a vector field. This problem was raised for the first time by Schlemmer et al. [8], who adapted the scalar moment invariants proposed by Mostafa and Psaltis [9] and Flusser [3,10] and designed invariants composed of geometric complex moments of the field. Schlemmer et al. used these invariants to detect specific patterns in a turbulent swirling jet flow. Rotation invariants from geometric complex moments have found several applications. Liu and Ribeiro [11] used them, along with a local approximation of the vector field by a polynomial, to detect singularities on meteorological satellite images showing wind velocity. Basically the same kind of rotation invariants were used by Liu and Yap [12] for the indexing and recognition of fingerprint images. Bujack et al. [13,14] studied the invariants of complex moments thoroughly, generalized the previous works, and showed that the invariants can be derived also by means of the field normalization approach. These authors demonstrated the use of the invariants in several pattern matching tasks including fluid dynamics simulation of a Kármán vortex street.

In all of the above-mentioned papers, despite of certain differences, the invariants are essentially based on standard geometric moments. It is well known from many studies of scalar images, that the geometric (and consequently the complex) moments have rather poor numerical properties, in particular they cannot be calculated in a stable way up to high orders [2]. This is caused by the fact that their basis functions $x^p y^q$ are not orthogonal. In scalar image analysis, this finding led to the design of invariants from orthogonal moments and from other orthogonal projections of the image (see, for instance, [2] for a survey). However, nothing like that has been published for vector fields so far.

In this paper, we introduce vector field invariants w.r.t. total rotation composed of orthogonal Gaussian–Hermite moments and of Zernike moments. We demonstrate that they have better numerical properties than the invariants of geometric/complex moments and they can be advantageously used in the vector field template matching tasks.

In the next section, we briefly recall Gaussian–Hermite moments. In Section 3, we show how the Gaussian–Hermite moments can be used for designing rotation invariants of vector fields. Section 4 introduces vector field invariants based on Zernike moments. Finally, numerical experiments and comparison are presented in Section 5.

2. Gaussian–Hermite polynomials and moments

Hermite polynomials are popular basis functions introduced by C. Hermite [15]. They have been widely used in signal analysis and in many other applications.

The Hermite polynomial of the n-th degree is defined as

$$H_n(x) = (-1)^n e^{x^2} \frac{\mathrm{d}^n}{\mathrm{d}x^n} e^{-x^2}. \tag{1}$$

Hermite polynomials are orthogonal on $(-\infty, \infty)$ with the weight $w(x) = e^{-x^2}$. For numerical calculations, Hermite polynomials can be evaluated in a fast and stable way by means of the three-term recurrence relation

$$H_n(x) = 2xH_{n-1}(x) - 2(n-1)H_{n-2}(x) \tag{2}$$

with the initialization $H_0(x) = 1$ and $H_1(x) = 2x$. If they are not modulated, they have a high range of values and poor localization, which makes them difficult to use directly for image description. To overcome this, we modulate Hermite polynomials with a Gaussian function and scale them. This normalization yields *Gaussian–Hermite (GH) polynomials*

$$\mathcal{H}_n(x, \sigma) = H_n(x/\sigma) e^{-\frac{x^2}{2\sigma^2}}. \tag{3}$$

In most cases, we work with *orthonormal* GH polynomials $\hat{\mathcal{H}}_n$, which differ from Eq. (3) just by the scalar factor:

$$\hat{\mathcal{H}}_n(x, \sigma) = \frac{1}{\sqrt{n! 2^n \sigma \sqrt{\pi}}} \mathcal{H}_n(x, \sigma). \tag{4}$$

As can be seen in Fig. 4, the GH polynomials have a range of values inside $(-1, 1)$. Although they are formally defined on $(-\infty, \infty)$, they are effectively localized into a small neighborhood of the origin controlled by σ.

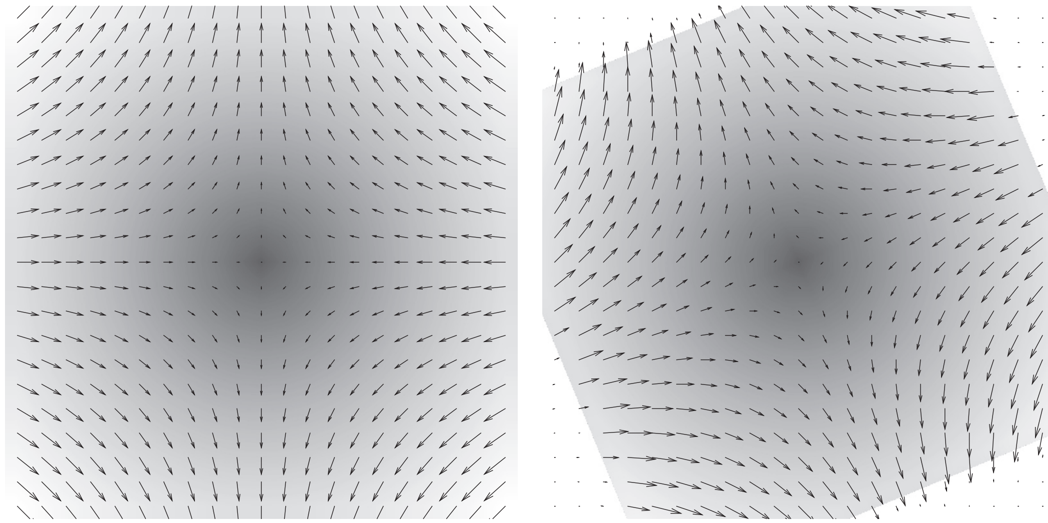

(a) (b)

Fig. 3. Vector field transformation: (a) original vector field, (b) its total rotation.

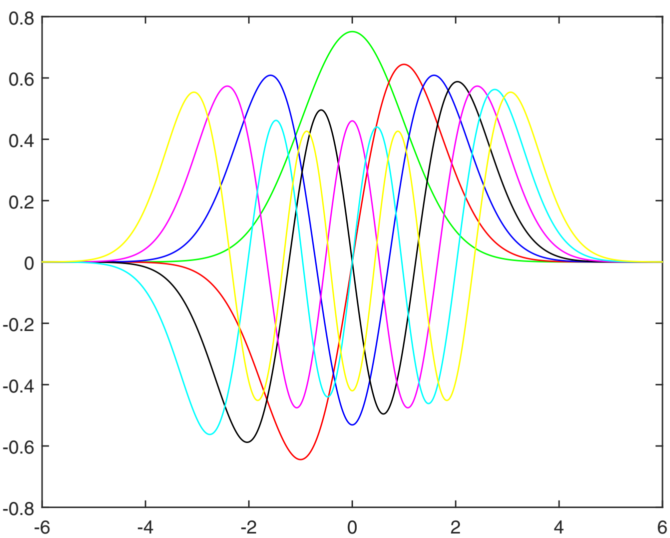

Fig. 4. The graphs of the Gaussian–Hermite polynomials up to degree 6 with $\sigma = 1$.

2D Gaussian–Hermite moments of a function *f*(*x*, *y*) are defined as

$$\hat{\eta}_{pq} = \int_{-\infty}^{\infty}\int_{-\infty}^{\infty} \hat{H}_p(x,\sigma)\hat{H}_q(y,\sigma)f(x,y)\mathrm{d}x\mathrm{d}y. \quad (5)$$

The GH moments were introduced to the image analysis community by Shen [16,17]. They were proved to be robust w.r.t. additive noise [18,19] and were successfully employed in several applications, such as in the detection of moving objects in videos [20], in license plate recognition [21], in image registration as landmark descriptors [4], in fingerprint classification [22], in face recognition [23,24], in 3D object reconstruction [25], and as directional feature extractors [26].

The main advantage of the GH moments for using in image processing is their simple transformation under a rotation of the spatial coordinates, as was discovered by Yang et al. [27,28] and employed to design GH rotation invariants of scalar images [29]. This property of the GH moments has been known as the *Yang's theorem*: If there exists rotation invariant $I(m_{p_1q_1}, m_{p_2q_2}, \dots, m_{p_dq_d})$ of geometric moments

$$m_{pq} = \int_{-\infty}^{\infty}\int_{-\infty}^{\infty} x^p y^q f(x,y)\mathrm{d}x\mathrm{d}y, \quad (6)$$

then the same function of the corresponding Hermite moments is also a rotation invariant (see [28] for the detailed proof). Furthermore, Gaussian weighting and scaling do not violate this property provided that the scale parameter σ is the same for x and y and that the normalizing coefficient has been set up as

$$\hat{\eta}_{pq} = \frac{1}{\sigma\sqrt{\pi(p+q)!2^{p+q}}}\int_{-\infty}^{\infty}\int_{-\infty}^{\infty} H_p(x,\sigma)H_q(y,\sigma)f(x,y)\mathrm{d}x\mathrm{d}y. \quad (7)$$

The Yang's theorem still holds well and the functional $I(\hat{\eta}_{p_1q_1}, \hat{\eta}_{p_2q_2}, \dots, \hat{\eta}_{p_dq_d})$ is a rotation invariant of the Gaussian–Hermite moments of scalar images [28].

In the next section, we adapt the Yang's theorem for vector fields and show how to construct GH invariants w.r.t. total rotation, which is the main theoretical contribution of the paper.

3. Gaussian–Hermite rotation invariants of vector fields

A vector field can be treated as a complex-valued function (or matrix in a discrete case)

$$\mathbf{f}(x,y) = f_1(x,y) + if_2(x,y),$$

which allows us to use the standard definition of moments. It holds, for arbitrary moment M_{pq},

$$M_{pq}^{(\mathbf{f})} = M_{pq}^{(f_1)} + iM_{pq}^{(f_2)},$$

where M_{pq} may stand for geometric, GH, or any other moment. Since the outer rotation (i.e. the rotation of the vector values) can be modeled as a multiplication of the vector field by a constant factor $e^{-i\alpha}$, any moment M_{pq} suffices

$$M'_{pq} = e^{-i\alpha}M_{pq}.$$

Hence, the GH moments are transformed exactly in the same way as the geometric moments. This allows us to formulate a generalization of the Yang's theorem to vector fields:

If there exists invariant to total rotation of a vector field $I(m_{p_1q_1}, m_{p_2q_2}, \dots, m_{p_dq_d})$ of geometric moments, then the same functional $I(\hat{\eta}_{p_1q_1}, \hat{\eta}_{p_2q_2}, \ldots, \hat{\eta}_{p_dq_d})$ of the Gaussian–Hermite moments is also an invariant.

Practical applicability of the Yang's vector-field theorem depends on our ability to find rotation invariant I composed of geometric moments (in practice, a single invariant is not sufficient and we are looking for a set providing a sufficient discriminability). That is, however, not easy. Already in the theory of moments of scalar images, it was shown [30] that the rotation invariants are hard to construct directly from the geometric moments. The same applies for vector fields, where the problem is even more difficult. In scalar moment invariants, the problem was overcome by using *complex moments*

$$c_{pq} = \int_{-\infty}^{\infty}\int_{-\infty}^{\infty}(x+iy)^p(x-iy)^q f(x,y)\mathrm{d}x\mathrm{d}y. \tag{8}$$

The complex moments change under the inner rotation by angle α simply as

$$c'_{pq} = e^{-i(p-q)\alpha}c_{pq} \tag{9}$$

(see [30] for the proof). Under a total rotation of a vector field, $c^{(\mathbf{f})}_{pq}$ fulfills

$$c^{(\mathbf{f}')}_{pq} = e^{-i\alpha}e^{-i(p-q)\alpha}\cdot c^{(\mathbf{f})}_{pq} = e^{-i(p-q+1)\alpha}\cdot c^{(\mathbf{f})}_{pq}. \tag{10}$$

The link between the geometric and the complex moments [30] (which is the same both for scalar and vector images)

$$c_{pq} = \sum_{k=0}^{p}\sum_{j=0}^{q}\binom{p}{k}\binom{q}{j}(-1)^{q-j}i^{p+q-k-j}m_{k+j,p+q-k-j} \tag{11}$$

yields the possibility of applying the Yang's theorem. When replacing the c_{pq}'s by the corresponding functions of the GH moments

$$d_{pq} = \sum_{k=0}^{p}\sum_{j=0}^{q}\binom{p}{k}\binom{q}{j}(-1)^{q-j}i^{p+q-k-j}\hat{\eta}_{k+j,p+q-k-j}, \tag{12}$$

the behavior under a total rotation must be preserved, which leads to

$$d^{(\mathbf{f}')}_{pq} = e^{-i(p-q+1)\alpha}\cdot d^{(\mathbf{f})}_{pq}. \tag{13}$$

Now we can cancel the rotation parameter by multiplication of proper powers of the d_{pq}'s. Let $\ell \geq 1$ and further let k_i, p_i, and q_i $(i = 1, \ldots, \ell)$ be non-negative integers such that

$$\sum_{i=1}^{\ell} k_i(p_i - q_i + 1) = 0.$$

Then,

$$I = \prod_{i=1}^{\ell} d^{k_i}_{p_iq_i} \tag{14}$$

is invariant with respect to total rotation of a vector field.

Eq. (14) may generate an infinite number of rotation invariants. It is desirable to work with an independent and complete subset (basis). The simplest possible basis can be obtained by

$$\Phi(p,q) \equiv d_{pq}d^{p-q+1}_{q_0p_0}, \tag{15}$$

where $p_0 - q_0 = 2$ and $d_{q_0p_0} \neq 0$. To get a complete system, we set by definition $\Phi(q_0, p_0) \equiv |d_{q_0p_0}|$ (note that $\Phi(q_0, p_0)$, if calculated from Eq. (15), would always equal one).

The choice of the basis is not unique and it is determined by the choice of $d_{q_0p_0}$, which is sometimes called the basic moment or the *normalizer*. The normalizer must be nonzero for all vector fields in the given experiment. If this condition was not fulfilled, the basis would lose its discrimination power. The construction of the basis requires special care if the fields in question exhibit certain symmetry, as we will see in the next section.

3.1. Symmetry issues

In moment-based pattern recognition, symmetric objects require special care when we define the invariants. Many moments are zero on objects that exhibit a certain symmetry. If they were used as a factor in a product, the invariant would become trivial on any object with the given type of symmetry. Trivial invariants do not provide any discriminability and only increase the dimensionality of the feature space, which may lead to a drop in performance. When we want to recognize different symmetric objects, the vanishing moments must be identified in advance and the trivial invariants need to be discarded from the system.

For rotation invariants of scalar images, the systematic analysis of this phenomenon was first presented in [31], where the authors showed the solution based on complex moments for objects with N-fold rotation symmetry. Vanishing of Gaussian–Hermite moments was studied later in [29], where the basis construction that prevents the use of the vanishing moments was proposed. The most general choice of the non-vanishing invariants of complex moments was proposed by Bujack [32], who introduced so-called flexible basis.

The problem of vanishing moments appears in case of vector fields, too. Unlike scalar images, the symmetry we have to investigate in the case of vector fields is that one which is related to the *total* rotation of the field. Let us define the notion of *total N-fold rotation symmetry*. The vector field $\mathbf{f}$ is said to be totally N-fold symmetric if it holds, for $\alpha = 2\pi/N$,

$$\mathbf{f}'(\mathbf{x}) \equiv \mathbf{R}_\alpha\mathbf{f}(\mathbf{R}_{-\alpha}\cdot\mathbf{x}) = \mathbf{f}(\mathbf{x}).$$

We may extend this definition also to $N = \infty$; then the equality must hold for any α.

If a vector field $\mathbf{f}$ is totally N-fold symmetric, then $d^{(\mathbf{f})}_{pq} = 0$ for any index pair p, q such that $(p - q + 1)/N$ is *not* an integer. This can be observed immediately from Eq. (13) if we set $\alpha = 2\pi/N$. Then, due to the symmetry of field $\mathbf{f}$, we get $d^{(\mathbf{f}')}_{pq} = d^{(\mathbf{f})}_{pq}$. This equality can be fulfilled only if $d^{(\mathbf{f})}_{pq} = 0$ or if $(p - q + 1)/N$ is integer.

We should take this proposition into account when designing invariants that are supposed to discriminate two vector fields with the same total N-fold symmetry. Instead of the basic invariants $\Phi(p, q)$ from Eq. (15), which may vanish, we create a non-trivial basis composed of the invariants

$$\Phi_N(p,q) \equiv d_{pq}d^{\frac{p-q+1}{N}}_{q_0p_0}, \tag{16}$$

where $(p - q + 1)/N$ is an integer and $p_0 - q_0 = N + 1$.

When considering a total radial symmetry $N = \infty$, the only non-vanishing invariants are

$$\Phi_\infty(p, p+1) \equiv d_{p,p+1}. \tag{17}$$

The described problem of invariants of symmetric fields is not marginal as many specific templates we search for often exhibit symmetry with respect to a total rotation. The symmetry must be identified in advance and the invariant basis should be chosen according to (16) or (17).

3.2. Flexible basis

However, in practice, symmetric patterns may not be exactly symmetric due to sampling errors. Even if we do not detect any zero moments, certain moments may be very close to zero. This may happen also for some non-symmetric patterns. If we choose such a numerically zero moment as a basic moment in (15), the resulting invariants may be unstable and vulnerable to noise. To overcome that, we may construct a so-called *flexible invariant basis* as follows. We relax the constraint given earlier on the indices

p_0 and q_0 by only requiring $p_0 - q_0 + 1 \neq 0$. We look for a "significantly non-zero" moment $d_{q_0 p_0}$ satisfying this constraint by calculating the average magnitude of all d_{pq}'s up to the given order. The lowest-order moment whose magnitude exceeds the average is then taken as the normalizer $d_{q_0 p_0}$ and the basis is constructed via

$$\Phi_{flex}(p,q) \equiv d_{pq} d_{q_0 p_0}^{\frac{p-q+1}{p_0-q_0-1}}. \tag{18}$$

There are $|p_0 - q_0 - 1|$ complex roots, so $\Phi_{flex}(p, q)$ is defined with a $|p_0 - q_0 - 1|$-ambiguity. Since all these solutions are dependent, it is sufficient to store a single value only (all of them should be, however, taken into account when comparing two patterns). To avoid working with the multiple roots, we can alternatively use the powers

$$\Pi(p,q) \equiv \Phi_{flex}(p,q)^{p_0-q_0-1} = d_{pq}^{p_0-q_0-1} d_{q_0 p_0}^{p-q+1}, \tag{19}$$

which are defined unambiguously.

The flexible basis avoids using close-to-zero moments but does not require a prior analysis of the symmetry. It may be used in any case; however for common non-symmetric and non-singular patterns the flexible basis provides the same discrimination power as the basis (15) (in many cases the chosen normalizer is exactly the same as in (15)).

4. Zernike rotation invariants of vector fields

Zernike polynomials were originally proposed to describe the diffracted wavefront in phase contrast imaging [33] and have found numerous applications in mathematics, optics, and imaging. Zernike moments (ZMs) [5] have become very popular in image analysis. They belong to the family of *radial moments*, along with the Pseudo–Zernike, Fourier–Mellin, Jacobi–Fourier, Chebyshev–Fourier, and other moments (see [2] for a survey)). Their main advantage comes from the fact that they are orthogonal on the unit disk, they keep their magnitude constant under an image rotation, and their phase change is simple and easy to eliminate. The latter property ensures a theoretically easy construction of rotation invariants of scalar images [6].

Zernike moment of degree n with repetition ℓ of vector field $\mathbf{f}$ is defined as

$$A_{n\ell} = \frac{n+1}{\pi} \int_0^{2\pi} \int_0^1 V_{n\ell}^*(r,\theta) \mathbf{f}(r,\theta) r \, \mathrm{d}r \mathrm{d}\theta, \tag{20}$$

where $n = 0, 1, 2, \dots$, $\ell = -n, -n+2, \dots, n$ and $V_{n\ell}(r, \theta)$ is the respective Zernike polynomial (see for instance [2] for its complete definition).

Under a total rotation of the field by α, ZMs are transformed as

$$A'_{n\ell} = A_{n\ell}\, e^{-i(\ell-1)\alpha}. \tag{21}$$

The rotation invariants of vector fields are then obtained by phase cancellation as

$$Z_{n\ell} = A_{n\ell} (A_{n_0 \ell_0})^{-(\ell-1)/(\ell_0-1)}, \tag{22}$$

where the normalizer should be chosen such that $\ell_0 \neq 1$ and $A_{n_0\ell_0} \neq 0$. If we choose $\ell_0 = 0$ or $\ell_0 = 2$, we avoid the complex roots and end up with simpler invariants

$$Z_{n\ell} = A_{n\ell} (A_{n_0 \ell_0})^{\pm(\ell-1)}. \tag{23}$$

5. Experiments

The goal of the experimental section is to compare the proposed orthogonal invariants of vector fields (both GH and ZM) to their competitors – the invariants composed of geometric/complex moments [2]. These invariants are formally defined by the same equation as (15), but complex moments c_{pq} are used in place of d_{pq}:

$$\Psi(p,q) \equiv c_{pq} c_{q_0 p_0}^{p-q+1} \tag{24}$$

and $\Psi(q_0, p_0) \equiv |c_{q_0 p_0}|$. A few special cases of the invariants (24) of low orders, without mentioning the general formula, were used in [8] and in the follow-up papers mentioned in the introduction. In fact, they perform the only method for template matching in vector fields published so far.

In the remainder of this paper, we will refer to the invariants given by Eq. (24) as the *geometric* invariants.[2]

In the first experiment, we demonstrate the main advantage of the orthogonal invariants – high numerical stability and low precision loss even for high-order invariants. The second and third experiments illustrate the application of the GH invariants in template matching in real vector fields.

5.1. Numerical precision

In this experiment, we evaluated numerical properties of GH, ZM and geometric moment invariants up to the order $p+q = 160$. It can be expected that high-order geometric moment invariants lose precision because they comprise very high and very low numbers. Since the GH moments can be calculated by the recurrence relation (2), the overflow and underflow effects should be less significant or even not present at all. The same is true for the Zernike moments. Due to their popularity, great effort has been made to develop efficient and numerically stable algorithms for their calculation [34–40]. In this experiment, we used an implementation of the recurrent *Kintner method* [2,34], which is like a gold standard in the ZM computation.

The evaluation is done by measuring the relative error of each invariant. We took a 365 × 451 vector field (obtained as a gradient field of the image of a hair, see Fig. 5), rotated it by $\pi/4$ using the total rotation, and calculated the relative error in percents as

$$\varepsilon_\Gamma(p,q) = 100 \cdot \frac{|\Gamma(p,q) - \Gamma'(p,q)|}{\Gamma(p,q)},$$

where $\Gamma(p, q)$ stands for the geometric/GH/ZM invariant and $\Gamma'(p, q)$ denotes the same invariant of the rotated field. Theoretically it should hold $\varepsilon = 0$ for any p, q, and Γ; the non-zero values are caused by the field resampling and by numerical errors of the moment calculations. This is why we used the rotation by $\pi/4$ – the relative errors are greater than for any other angle and allow to observe the differences between the three types of the invariants clearly.

The relative errors of the geometric invariants are visualized in Fig. 6 using the color map on the right. It is worth noting that the invariants are well defined only in a strip along the diagonal $p = q$. Outside the colored area, the Matlab code yielded NaN values when calculating the invariants. This illustrates the limited possibility of working with the geometric invariants if $p - q > 20$ and $p, q > 80$ (the particular numbers depend on the given vector field).

The relative errors of the GH invariants and the ZM invariants are visualized in the same way in Fig. 7 and in Fig. 8, respectively. The main difference, which is apparent at first sight, is that all investigated invariants are valid, there have been no NaN's in the

[2] This terminology originates from the fact that the complex moments are simple functions of geometric moments, the most elementary moments. Sometimes they are called *monomial* invariants because they are based on the monomial basis functions.

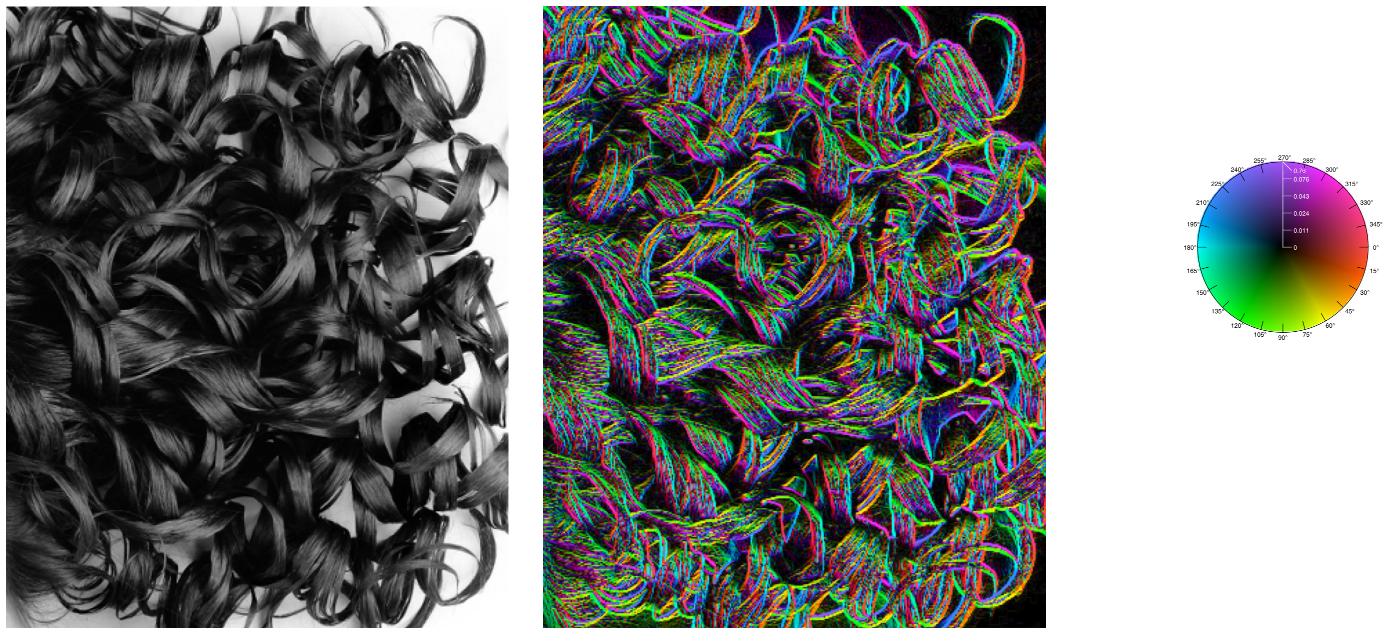

(a) (b) (c)

Fig. 5. Hair image: (a) the original, (b) the gradient field, and (c) the colormap for gradient visualization. The brightness corresponds to the magnitude and the hue to the direction of the gradient.

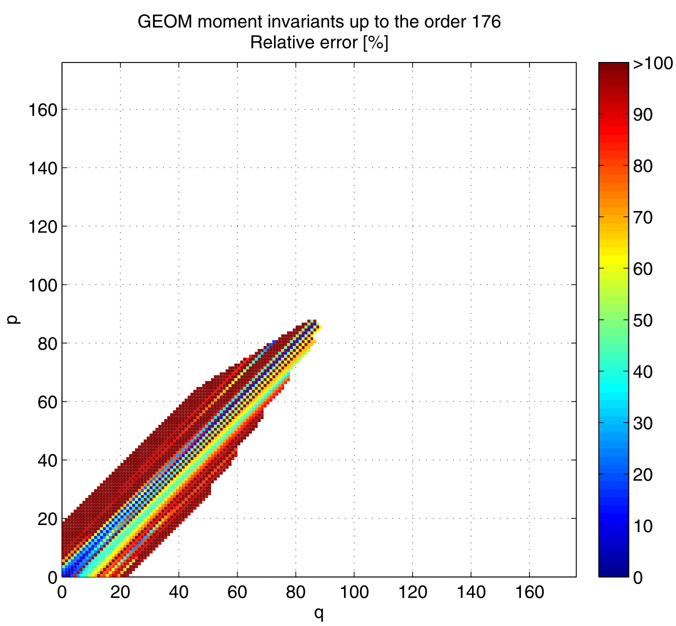

Fig. 6. Relative errors of the geometric invariants. White area corresponds to NaN values of the invariants.

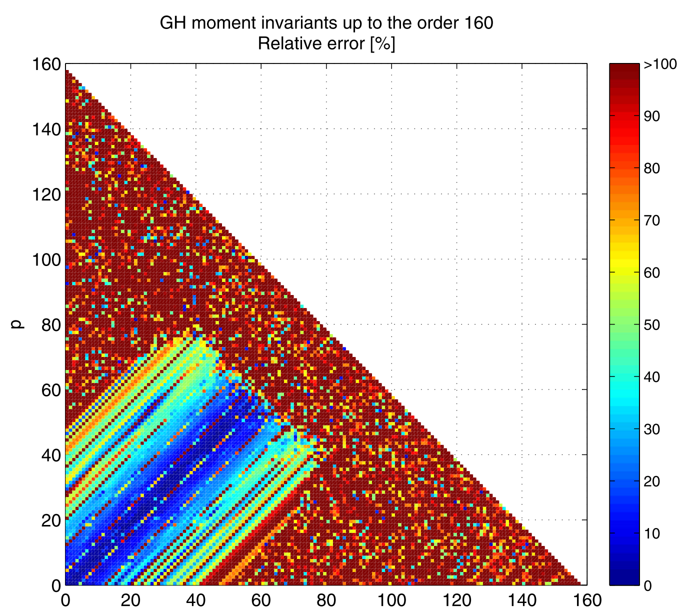

Fig. 7. Relative errors of the Gaussian–Hermite invariants.

calculations. To compare the relative errors in the valid region, we calculated element-wise the ratios

$$\varrho_1(p,q) = \frac{\varepsilon(geometric)}{\varepsilon(GH)},$$

$$\varrho_2(p,q) = \frac{\varepsilon(geometric)}{\varepsilon(ZM)},$$

and

$$\varrho_3(p,q) = \frac{\varepsilon(GH)}{\varepsilon(ZM)}.$$

They are visualized in Figs. 9–11. While the calculation of ϱ_1 is straightforward, the definition of ϱ_2 and ϱ_3 may not be unique, because the second index of the Zernike moment expresses the angular repetition factor while both indices of the geometric/GH moments are the degrees of the basis polynomials. A reasonable way, which we employed here, of comparing the geometric/GH moments to the ZMs, is to link the indices p, q of geometric/GH moments to the indices $p+q$, $p-q$ of the ZMs. The yellow-red color map is used for $\varrho > 1$, light green is neutral ($\varrho = 1$) and green-blue stands for $\varrho < 1$ (to keep the same range on both sides, the values of $\varrho > 1$ were displayed as $2 - 1/\varrho$). The vast majority of indices

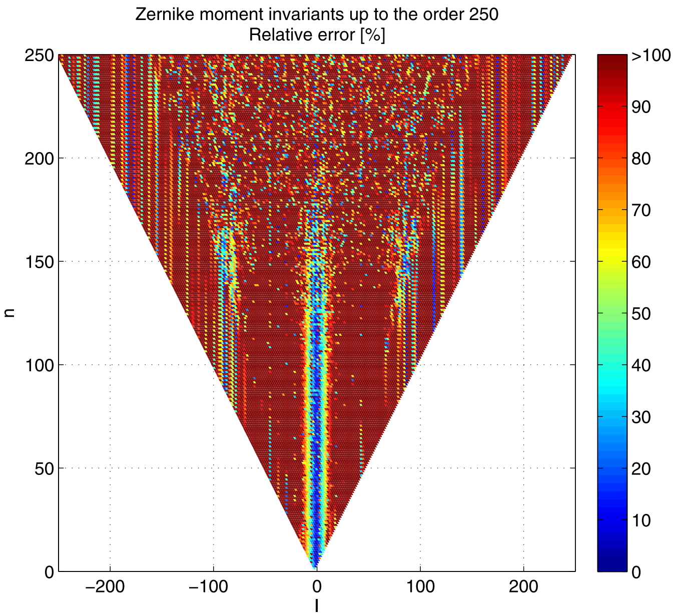

Fig. 8. Relative errors of the Zernike moment invariants.

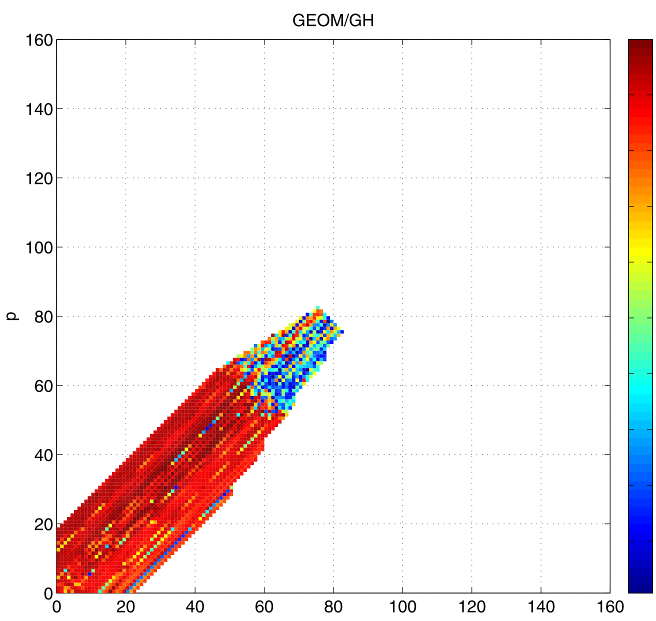

Fig. 9. The ratio of the relative errors ϱ_1.

(p, q) (precisely in 85%), satisfies $\varrho_1 > 1$, which means the relative error of the geometric invariants is higher than that of the GH invariants. The mean value of ϱ_1 is 7.3 and the median equals 4.3, which clearly illustrates the higher stability of the GH invariants. The behavior of ϱ_2 is similar, although the dominance of the ZMs is not as prominent.

The quantitative comparison between the GH and ZM invariants is expressed by ϱ_3. In the central strip area, the GH invariants are more stable (the mean value of ϱ_3 is 0.8, the median is 0.65). Outside this area, ϱ_3 looks like a close-to-zero-mean random noise, which shows there is no significant difference between the GH and ZM invariants in this range of the indices.

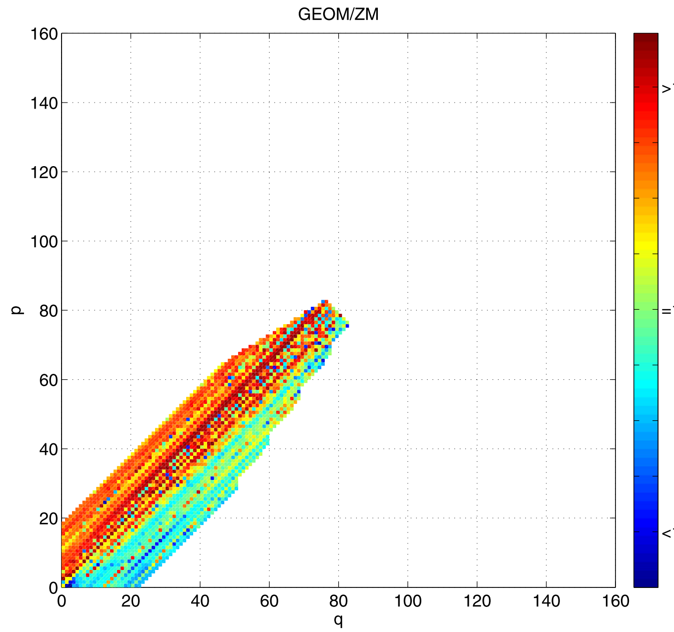

Fig. 10. The ratio of the relative errors ϱ_2.

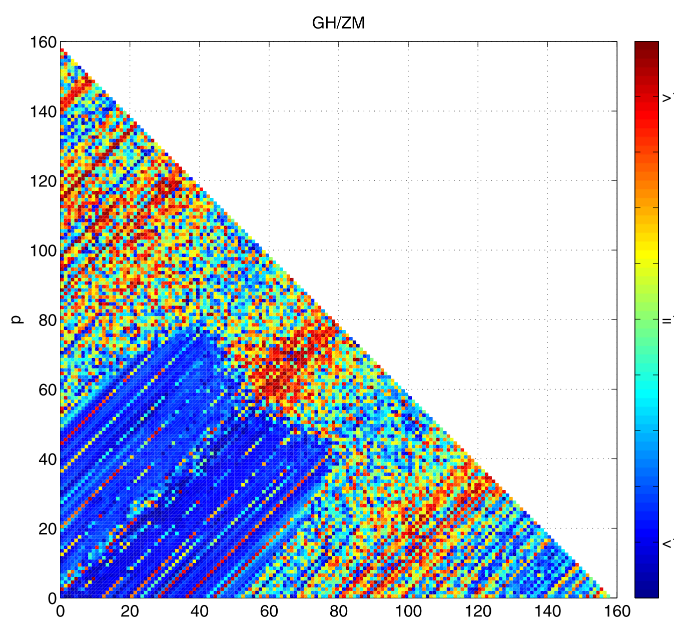

Fig. 11. The ratio of the relative errors ϱ_3.

5.2. Template matching in a gradient field

In this experiment we demonstrate the use of the GH invariants for template matching, i.e. in the task they have been designed for and where they are supposed to be applied in practice. As the test vector field, we again used the gradient of the hair image, see Fig. 5. We chose this particular photograph to make the matching challenging. On one hand, the picture is rich in edges so there are no large regions of a constant gradient; on the other hand there are many patches similar to each other, which makes the matching non-trivial.

We randomly extracted 1000 circular templates of the radius 20 pixels from the gradient field, rotated them by random angles, and matched them against the original field. The matching was carried out by searching for the minimum ℓ_2-distance in the space

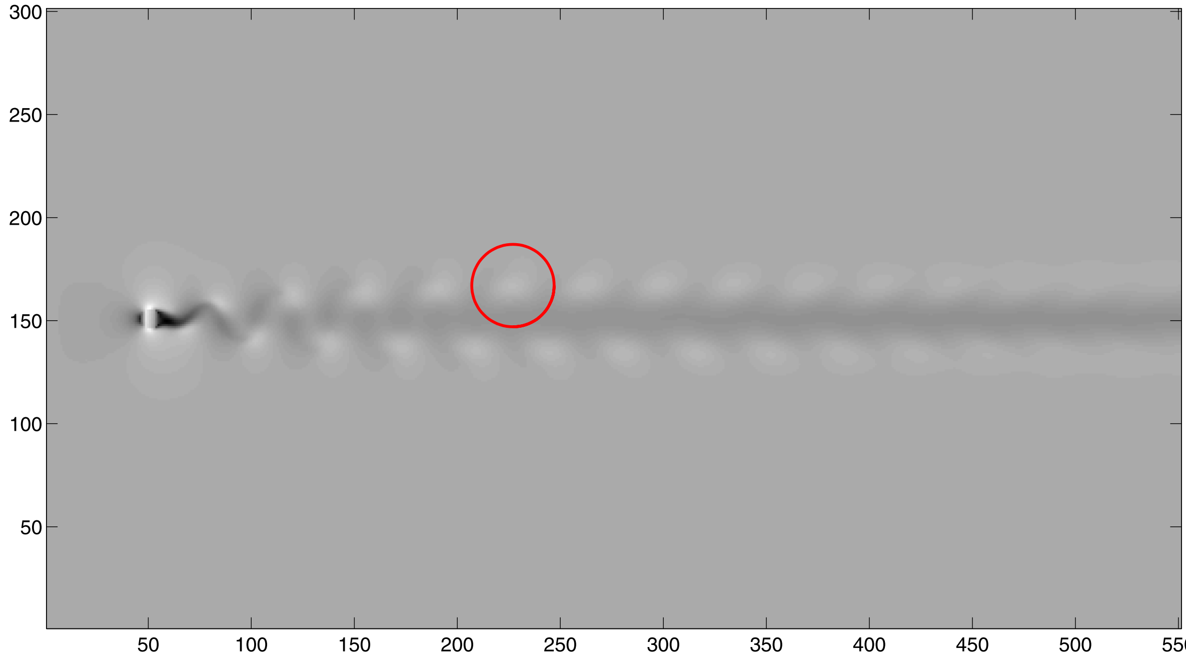

Fig. 12. The Kármán vortex street with the selected template.

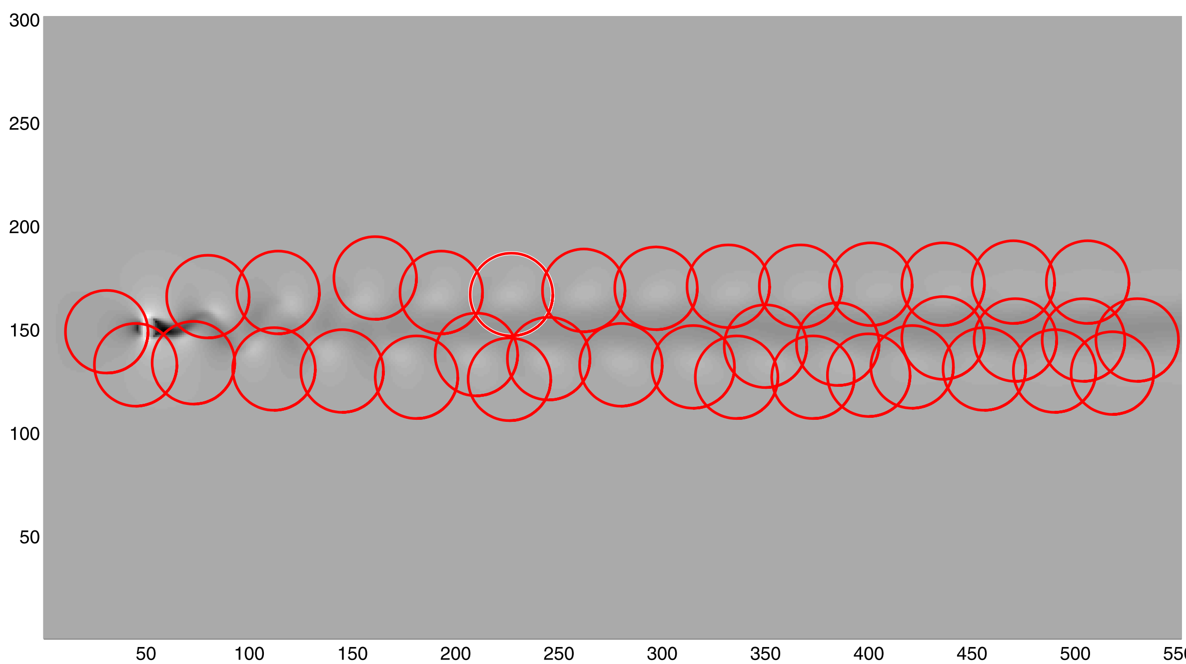

Fig. 13. The matching vortices when only the GH invariants up to the fourth order have been employed.

of the invariants between the template and all field patches of the same size. We encountered two kinds of errors which we call ”small” and ”gross”. An error is considered ”small” if it is less than 10 pixels (measured as the Euclidean distance from the ground-truth location). These errors are governed by a Rayleigh distribution $R(x;\sigma)$ [41] (provided that the errors in horizontal and vertical directions are independent, normally distributed random variables with the same variance), whose density is

$$R(x;\sigma) = \frac{x}{\sigma^2} e^{-\frac{x^2}{2\sigma^2}}. \tag{25}$$

The mean value of the distribution, which we used to quantify the small errors, is $\sigma\sqrt{\pi/2}$.

The “gross” error means the template was found at a completely wrong place, usually because there was a similar patch at that position. Since in most applications the errors are considered equally serious if they are, let us say, 50 or 500 pixels (in both cases, the location found is totally wrong and the position cannot be refined by searching within a neighborhood), we only count the number of these gross errors to evaluate the matching.

We matched each template by eight different invariants for comparison. We used the vector-field GH invariants up to the orders four and six to illustrate the contribution of higher orders. To show the differences in numerical stability, we did the same with the vector-field invariants composed of complex (geometric) moments [2]. Finally, we converted the vector values to magnitudes

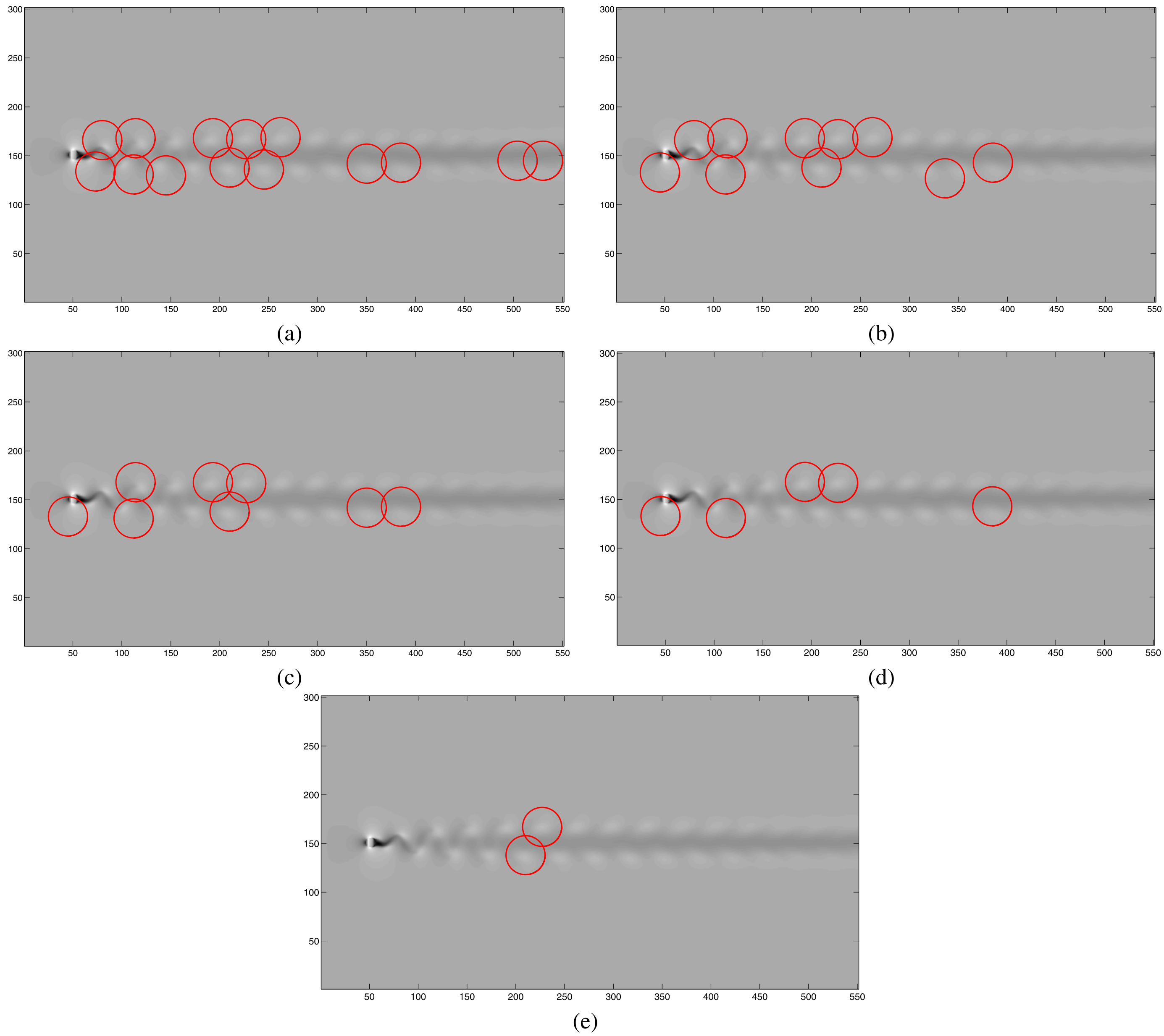

Fig. 14. The matching vortices when also higher-order GH invariants have been used. The higher orders obviously yield less matching results: (a) fifth order, (b) seventh order, (c) ninth order, (d) eleventh order, and (e) thirteenth order.

Table 1
The number of gross errors (NGE) and the mean small errors (MSE) out of 1000 trials in the experiment with the template matching in the gradient field.

Features	4th order		6th order	
	NGE	MSE	NGE	MSE
GH vector	114	0.504	75	0.401
CM vector	360	1.157	282	0.836
GH scalar	391	0.748	176	0.624
CM scalar	745	1.497	647	1.070

and used traditional scalar image invariants (both GH and CM) acting on magnitudes only to match the templates. This shows that the vector field template matching cannot be reduced to scalar image matching without a loss of performance. The results are summarized in Table 1. It can be seen clearly, that the vector field GH invariants outperform the other three methods significantly, both in the number of gross errors as well as in the mean value of the small ones. At the same time, we can observe an improvement of the performance of all methods when the 6-th order moments were used.

5.3. Template matching in a fluid flow field

In this experiment, we demonstrate the applicability of the proposed technique in an important problem from fluid dynamics engineering – vortex detection in a fluid flow vector field. We used the field showing the Kármán vortex street, which is a repeating pattern of swirling vortices caused by the flow of a fluid around blunt bodies. In the Kármán pattern, we can see several vortices arranged into two rows. The orientation of the "street" is given by the main flow direction and is generally not known a priori. A patch with a typical vortex is used as a template. In this task we used a vortex from the upper row (see Fig. 12), but generally, the template may be extracted from another similar field. To sim-

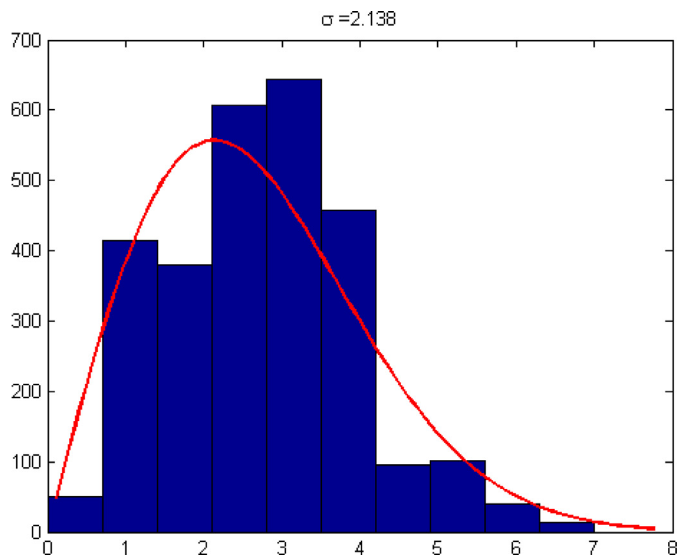

Fig. 15. The histogram of absolute errors (in pixels) of the vortex localization (the bar graph) with the fitted Rayleigh distribution superimposed (the curve).

ulate this, we rotated the template by 30 degrees. The task is to find all vortices of a similar shape regardless of their orientation. The search is performed in the space of the rotation invariants. Unlike the previous experiment, we search for all local minima of ℓ_2-distance below a user-defined threshold.

Such a task definition is rather "soft", because it specifies neither the significance of the vortices to be detected nor the required degree of similarity with the template. As we can see, the results may be controlled by the number/order of the invariants we use.[3]

In Fig. 13, we can see the matching results when only the invariants up to the fourth order have been employed. Almost all vortices, existing in the field, were detected. The detection of the vortices in the bottom row requires special care, because they are flipped comparing to the upper row. The GH invariants are transformed under a mirroring w.r.t. an arbitrary line as

$$\bar{\Phi}(p,q) = \Phi(p,q)^*. \tag{26}$$

Hence, the real part of $\Phi(p, q)$ keeps its value, but the imaginary part should be taken with an opposite sign. If we want to detect both kinds, the absolute value of the imaginary part should be used.

As we increased the order of the invariants, we identified only those vortices, which are more similar to the template (see Fig. 14). Note that the results does not necessarily form a nested sequence because the degree of similarity may not be monotonic with the order. This process terminated at the order 14, where only a single vortex, the one identical with the template, was found.

The previous experiment was carried out on a single vector field with a few templates. In order to perform an objective error analysis, we used a 300-frame video, showing the time-development simulation of the Kármán street. We used the same vortex template as before and matched it to each frame individually. To ensure independency, no information from the previous frames was used. We employed the GH invariants up to the fourth order. In each frame, the algorithm identified 21 or 22 vortices, which are similar to the template. The video with the vortex tracking is at [42]. To evaluate the accuracy, we measured the localization error of each vortex in each frame. The ground truth positions were deduced from the fluid mechanics theory, which guarantees (under ideal conditions) the equidistant placement of the vortices (this assumption, however, works only in the first half of the street; the second half behaves differently and the ground-truth positions could not be estimated there). The ground-truth positions of the first two vortices were detected manually. We measured the absolute localization errors of all templates in the first half of each frame, so we obtained about 3000 random values, which should exhibit a Rayleigh distribution. We estimated its parameter σ and, consequently, the mean of the absolute errors (see Fig. 15 for the error histogram fitted with the Rayleigh curve). We obtained $\sigma = 2.138$, which yields the mean $m = \sigma\sqrt{\pi/2} = 2.68$. The actual mean localization error is probably even smaller because our Kármán street does not behave exactly as the ideal one and the error we have measured contains not only the localization error but also the error between the ideal and actual Kármán street.

6. Conclusion

The paper introduced rotation invariants of vector fields, which are functions of orthogonal moments. Vector fields behave differently from graylevel and color images under spatial transformations and traditional scalar invariants cannot be efficiently used for recognition.

Although vector-field invariants can be from simple geometric moments [2], in this paper we demonstrated that the use of orthogonal moments provides significantly higher numerical stability than the stability of geometric/complex moment invariants. We tested two popular kinds of orthogonal moments – Gaussian–Hermite and Zernike moments. Although they are distinct from one another in their nature (the GH moments are orthogonal on a square, while the Zernike moments are orthogonal on a disk), both can be employed as the building blocks of the invariants. The stability of the GH invariants was slightly better in our experiments, but the difference was not significant and each kind has its own pros and cons, implied by their different areas of orthogonality. We demonstrated their performance in template matching in a gradient field and in a vortex detection in a fluid flow vector field. Comparing to vector-field invariants from non-orthogonal moments and to scalar image invariants, the proposed technique achieved significantly better results.

The paper was focused solely on rotational invariance. Translational invariance is irrelevant in template matching (it could be ensured by using central moments if needed). Invariance to total scaling of the vector field is formally not difficult to achieve – we can just follow the idea of *variable modulation* of the GH moments, which was proposed for scalar images by Yang et al. [43] and which can be modified for vector fields easily. Dealing with scaled templates brings, however, another problem. Since it is not clear how large the corresponding neighborhood should be, one has to test several sizes in a reasonable interval, which increases the computational time.

Acknowledgments

This work was supported by the National Natural Science Foundation of China (Grant No. 61502389), by the Fundamental Research Funds for the Central Universities (Grant No. 3102015ZY047), by Science Foundation of Ministry of Education (Grant No. G2016001 and No. X2017016), and by Scientific and Technological Project in Shaanxi Province (Grant No. 2016GY-070). It was also supported by the Czech Science Foundation (Grant No. GA15-16928S), and by the Grant Agency of the Czech Technical University (Grant No. SGS15/214/OHK4/3T/14). This work is published under LA-UR-17-26797. It was supported by the National

[3] The number of matches may be influenced also by the choice of the threshold. To eliminate this influence, we used thresholds of the same significance in each moment order and the same thresholds in each run of the experiment.

Nuclear Security Administration (NNSA) Advanced Simulation and Computing (ASC) Program.

We thank Professor Mario Hlawitschka for providing the Kármán vortex street data.

Access to computing and storage facilities owned by parties and projects contributing to the National Grid Infrastructure MetaCentrum provided under the programme "Projects of Large Research, Development, and Innovations Infrastructures" (CESNET LM2015042), is greatly appreciated.

References

[1] A. Goshtasby, Template matching in rotated images, IEEE Trans. Pattern Anal. Mach. Intell. 7 (3) (1985) 338–344.
[2] J. Flusser, T. Suk, B. Zitová, 2D and 3D Image Analysis by Moments, Wiley, Chichester, U.K., 2016.
[3] J. Flusser, On the independence of rotation moment invariants, Pattern Recognit. 33 (9) (2000) 1405–1410.
[4] B. Yang, T. Suk, M. Dai, J. Flusser, 2D and 3D image analysis by Gaussian-Hermite moments, in: G.A. Papakostas (Ed.), Moments and Moment Invariants - Theory and Applications, Gate to Computer Science and Research, Vol. 1, Science Gate Publishing, 2014, pp. 143–173, doi:10.15579/gcsr.vol1.
[5] M.R. Teague, Image analysis via the general theory of moments, J. Opt. Soc. Am. 70 (8) (1980) 920–930.
[6] Å. Wallin, O. Kübler, Complete sets of complex Zernike moment invariants and the role of the pseudoinvariants, IEEE Trans. Pattern Anal. Mach. Intell. 17 (11) (1995) 1106–1110.
[7] P.-T. Yap, X. Jiang, A.C. Kot, Two-dimensional polar harmonic transforms for invariant image representation, IEEE Trans. Pattern Anal. Mach. Intell. 32 (7) (2010) 1259–1270.
[8] M. Schlemmer, M. Heringer, F. Morr, I. Hotz, M.-H. Bertram, C. Garth, W. Kollmann, B. Hamann, H. Hagen, Moment invariants for the analysis of 2D flow fields, IEEE Trans. Vis. Comput. Graph 13 (6) (2007) 1743–1750.
[9] Y.S. Abu-Mostafa, D. Psaltis, Recognitive aspects of moment invariants, IEEE Trans. Pattern Anal. Mach. Intell. 6 (6) (1984) 698–706.
[10] J. Flusser, On the inverse problem of rotation moment invariants, Pattern Recognit. 35 (12) (2002) 3015–3017.
[11] W. Liu, E. Ribeiro, Detecting singular patterns in 2-D vector fields using weighted Laurent polynomial, Pattern Recognit. 45 (11) (2012) 3912–3925.
[12] M. Liu, P.-T. Yap, Invariant representation of orientation fields for fingerprint indexing, Pattern Recognit. 45 (7) (2012) 2532–2542.
[13] R. Bujack, I. Hotz, G. Scheuermann, E. Hitzer, Moment invariants for 2D flow fields using normalization, in: Pacific Visualization Symposium, PacificVis'14, IEEE, 2014, pp. 41–48.
[14] R. Bujack, M. Hlawitschka, G. Scheuermann, E. Hitzer, Customized TRS invariants for 2D vector fields via moment normalization, Pattern Recognit. Lett. 46 (1) (2014) 46–59.
[15] C. Hermite, Sur un nouveau développement en série des fonctions, Vol. 58, Gauthier-Villars, 1864. (in French)
[16] J. Shen, Orthogonal Gaussian-Hermite moments for image characterization, in: D.P. Casasent (Ed.), Intelligent Robots and Computer Vision XVI: Algorithms, Techniques, Active Vision, and Materials Handling, 3208, SPIE, 1997, pp. 224–233.
[17] J. Shen, W. Shen, D. Shen, On geometric and orthogonal moments, Int. J. Pattern Recognit. Artif. Intell. 14 (7) (2000) 875–894.
[18] L. Wang, Y. Wu, M. Dai, Some aspects of Gaussian-Hermite moments in image analysis, in: L.P. Suresh, S.S. Dash, B.K. Panigrahi (Eds.), Third International Conference on Natural Computation ICNC'07, Advances in Intelligent Systems and Computing, Vol. 2, IEEE, 2007, pp. 450–454.
[19] J. Shen, W. Shen, D. Shen, On geometric and orthogonal moments, in: J. Shen, P.S.P. Wang, T. Zhang (Eds.), Multispectral Image Processing and Pattern Recognition, Machine Perception Artificial Intelligence, Vol. 44, World Scientific Publishing, 2001, pp. 17–36.
[20] Y. Wu, J. Shen, Properties of orthogonal Gaussian-Hermite moments and their applications, EURASIP J. Appl. Signal Process. (4) (2005) 588–599.
[21] X. Ma, R. Pan, L. Wang, License plate character recognition based on Gaussian-Hermite moments, in: Second International Workshop on Education Technology and Computer Science ETCS'10, 3, IEEE, 2010, pp. 11–14.
[22] L. Wang, M. Dai, Application of a new type of singular points in fingerprint classification, Pattern Recognit. Lett. 28 (13) (2007) 1640–1650.
[23] S. Farokhi, U.U. Sheikh, J. Flusser, B. Yang, Near infrared face recognition using Zernike moments and Hermite kernels, Inf. Sci. (Ny) 316 (2015) 234–245.
[24] N. Belghini, A. Zarghili, J. Kharroubi, 3D face recognition using Gaussian–Hermite moments, Int. J. Comput. Appl. Special Issue Softw. Eng. Databases Expert Syst. SEDEX (1) (2012) 1–4.
[25] B. Yang, J. Flusser, T. Suk, 3D rotation invariants of Gaussian–Hermite moments, Pattern Recognit. Lett. 54 (1) (2015) 18–26.
[26] B. Yang, J. Flusser, T. Suk, Steerability of Hermite kernel, Int. J. Pattern Recognit. Artif. Intell. 27 (4) (2013) 1–25.
[27] B. Yang, M. Dai, Image analysis by Gaussian–Hermite moments, Signal Process. 91 (10) (2011) 2290–2303.
[28] B. Yang, G. Li, H. Zhang, M. Dai, Rotation and translation invariants of Gaussian–Hermite moments, Pattern Recognit. Lett. 32 (2) (2011) 1283–1298.
[29] B. Yang, J. Flusser, T. Suk, Design of high-order rotation invariants from Gaussian–Hermite moments, Signal Process. 113 (1) (2015) 61–67.
[30] J. Flusser, T. Suk, B. Zitová, Moments and Moment Invariants in Pattern Recognition, Wiley, Chichester, U.K., 2009.
[31] J. Flusser, T. Suk, Rotation moment invariants for recognition of symmetric objects, IEEE Trans. Image Process. 15 (12) (2006) 3784–3790.
[32] R. Bujack, J. Flusser, Flexible basis of rotation moment invariants, in: V. Skala (Ed.), International Conferences in Central Europe on Computer Graphics, Visualization and Computer Vision WSCG'17, 2017.
[33] F. Zernike, Beugungstheorie des Schneidenverfarhens und seiner verbesserten Form, der Phasenkontrastmethode, Physica 1 (7) (1934) 689–704. (in German)
[34] E.C. Kintner, On the mathematical properties of Zernike polynomials, J. Mod. Opt. 23 (8) (1976) 679–680.
[35] A. Prata, W.V.T. Rusch, Algorithm for computation of Zernike polynomials expansion coefficients, Appl. Opt. 28 (4) (1989) 749–754.
[36] S.-K. Hwang, W.-Y. Kim, A novel approach to the fast computation of Zernike moments, Pattern Recognit. 39 (11) (2006) 2065–2076.
[37] J. Gu, H.Z. Shu, C. Toumoulin, L.M. Luo, A novel algorithm for fast computation of Zernike moments, Pattern Recognit. 35 (12) (2002) 2905–2911.
[38] C.-W. Chong, P. Raveendran, R. Mukundan, An efficient algorithm for fast computation of pseudo-Zernike moments, Int. J. Pattern Recognit. Artif. Intell. 17 (06) (2003) 1011–1023.
[39] S.O. Belkasim, M. Ahmadi, M. Shridhar, Efficient algorithm or fast computation of Zernike moments, J. Franklin Inst. 333(B) (4) (1996) 577–581.
[40] K.M. Hosny, Fast computation of accurate Zernike moments, J. Real-Time Image Process. 3 (1) (2010) 97–107.
[41] Wikipedia, https://en.wikipedia.org/wiki/Rayleigh_distribution#cite_note-1 last watch 2017.
[42] B. Yang, J. Kostková, J. Flusser, T. Suk, R. Bujack, 2017a https://drive.google.com/drive/folders/0B7eg_EHhe-jSOHlvWnRLYThhYjg.
[43] B. Yang, J. Kostková, J. Flusser, T. Suk, Scale invariants from Gaussian–Hermite moments, Signal Process. 132 (2017) 77–84.

Bo Yang received the M.Sc. degree in Control Science and Engineering from the Northwestern Polytechnical University, Xi'an, China in 2007, his Ph.D. degree in Image Science from the University of Bordeaux 3, France, in 2012. He was a post-doctoral at the Institute of Information Theory and Automation, Prague, in Czech Republic from 2012 to 2014. Currently, he works as a lecturer in the Northwestern Polytechnical University at Xi'an. His research interests include image processing and pattern recognition with a particular focus on applications of orthogonal polynomials.

Jitka Kostkova received the M.Sc. degree in Applied Mathematical Stochastic Methods from the Czech Technical University, Faculty of Nuclear Science and Physical Engineering, Prague, Czech Republic, in 2015. Currently, she is a PhD student in Mathematical Engineering and tutors undergraduate courses on mathematical analysis at the same university. Jitka Kostkova's research interest is focused on moments and moment invariants.

Jan Flusser received the M.Sc. degree in mathematical engineering from the Czech Technical University, Prague, Czech Republic, in 1985, the Ph.D degree in computer science from the Czechoslovak Academy of Sciences in 1990, and the DrSc. degree in technical cybernetics in 2001. Since 1985 he has been with the Institute of Information Theory and Automation, Czech Academy of Sciences, Prague. In 1995–2007, he was holding the position of a head of Department of Image Processing. Since 2007 he has been a Director of the Institute. He is a full professor of computer science at the Czech Technical University, Faculty of Nuclear Science and Physical Engineering, and at the Charles University, Faculty of Mathematics and Physics, Prague, Czech Republic, where he gives undergraduate and graduate courses on Digital Image Processing, Pattern Recognition, and Moment Invariants and Wavelets. Jan Flusser's research interest covers moments and moment invariants, image registration, image fusion, multichannel blind deconvolution, and super-resolution imaging. He has authored and coauthored more than 200 research publications in these areas, including the monographs *Moments and Moment Invariants in Pattern Recognition* (Wiley, 2009) and *2D and 3D Image Analysis by Moments* (Wiley, 2016). In 2007 Jan Flusser received the Award of the Chairman of the Czech Science Foundation for the best research project and won the Prize of the Academy of Sciences of the Czech Republic for the contribution to image fusion theory. In 2010, he was awarded by the SCOPUS 1000 Award. He received the Felber Medal of the Czech Technical University for excellent contribution to research and education in 2015 and the Academic Premium of the Czech Academy of Sciences for outstanding researchers in 2017.

Tomas Suk received the M.Sc. degree in electrical engineering from the Czech Technical University, Faculty of Electrical Engineering, Prague, Czech Republic, in 1987 and the Ph.D degree in computer science from the Czechoslovak Academy of Sciences in 1992. Since 1991 he has been a researcher with the Institute of Information Theory and Automation, Czech Academy of Sciences, Prague. He has authored 15 journal papers and more than 30 conference papers. Tomas Suk's research interests include digital image processing, pattern recognition, image filtering, invariant features, moment-based and point-based invariants, spatial transformations of images, and applications in remote sensing, astronomy, botany, medicine, and computer vision. In 2002 Tomas Suk received the Otto Wichterle Premium of the Czech Academy of Sciences for excellent young scientists.

Roxana Bujack graduated as M.Sc. in mathematics at Leipzig University in Germany in 2010. Then, she received her B.Sc. and her Ph.D. in computer science in the Image and Signal Processing Group at Leipzig University. She worked as a postdoctoral researcher at IDAV at the University of California, Davis in the USA and at the Computer Graphics and HCI Group at the Technical University Kaiserslautern. Currently, she is a staff scientist in the Data Science at Scale Team at Los Alamos National Laboratory. Her research interests include visualization, pattern recognition, vector fields, moment invariants, Lagrangian flow representations, image processing, big data, and Clifford analysis.